

激发端口可电切换的单向类电磁诱导透明效应

冉佳^{1,2,3*}, 张思文¹, 王文昌¹, 郝宏刚^{1,3}, 谭菲¹, 陈永强⁴¹重庆邮电大学光电工程学院, 重庆 400065;²重庆邮电大学光电信息感测与传输技术重庆市重点实验室博士后科研工作站, 重庆 400065;³重庆邮电大学高等研究院, 重庆 400065;⁴苏州科技大学物理科学与技术学院, 江苏 苏州 215009

摘要 具有非对称电磁响应特性的单向类电磁诱导透明效应(EIT-like)是超材料领域重要的研究课题之一,然而目前缺少可动态切换的单向EIT-like实现手段。基于此,提出一种利用二端口的微带谐振腔与两个开口谐振环之间的耦合作用构造单向EIT-like的方法,只有特定端口能够激发出EIT-like效应,其非对称反射系数对比度达到98.7%。在此基础上,结合可调的复合左右手传输线,对微带谐振腔与开口谐振环间的耦合情况进行动态调控,从而改变单向EIT-like的激发端口,实现了激发端口可电切换的单向EIT-like,推动EIT-like在光学存储、光调制、传感等方面的应用。

关键词 类电磁诱导透明; 复合左右手传输线; 微带谐振腔; 开口谐振环; 单向反射

中图分类号 O436

文献标志码 A

DOI: 10.3788/AOS230774

1 引言

电磁诱导透明效应(EIT)是多能级原子系统在外部光场作用下产生的一种特殊量子干涉效应,透射型EIT在吸收频带中会出现明显的透射窗口,反射型EIT在强反射频带中会出现低反射谷,两种形式都伴随强烈色散和慢波效应,在非线性光学和量子存储中有着广泛的应用^[1-5]。然而,在原子系统中实现EIT通常需要高功率激光源和极低的温度条件,严重阻碍了EIT的实际运用推广^[6-7]。超材料是一类人工结构性材料,其由具有强电磁响应特性的谐振单元周期性排布而成,能够灵活调控电磁波的相位、极化、振幅等,为EIT在低成本、高稳定性运行环境中的实现提供了可靠的平台。原子系统的EIT^[8-9]是量子相消干涉效应导致的,Zhang等^[10]在2008年通过超材料中电磁谐振单元之间的耦合作用实现光学系统的EIT-like效应,以模拟原子系统的EIT效应,能够获得与原子系统中EIT效应类似的传输特征。利用波导系统中双谐振子之间的耦合作用,在近红外等多个频段也实现了EIT-like效应^[11-12]。EIT-like效应能够在室温下实现强烈色散^[13],在传感器^[14-18]、光存储器^[19]、调制器^[20]、光开关^[21]和非互易传输设备^[22]的研究中受到了广泛的关注。

单向EIT-like是一种特殊的EIT-like效应,只有从特定的端口入射电磁波,才能激发出EIT-like效应。

单向EIT-like在实现定向反射方面发挥着重要的作用,为单向隐身(unidirectional invisibility)提供了新的实现思路^[23-24],同时在海洋勘探等方面也拥有重要的应用潜力^[25]。EIT-like效应依赖于明模(bright mode)和暗模(dark mode)之间的耦合作用。Hu等^[26]在微波波段,利用微带线谐振腔构造了非对称分布的驻波场,并通过在谐振腔中集成两个开口谐振环(SRRs)来构建明、暗模式,从不同端口入射的波激发出的驻波场分布是不同的,导致SRRs与入射波的耦合情况也不一样,实现了非对称的反射型单向EIT-like效应。文献^[23-24, 26]也提出了诸多单向EIT-like效应的实现方案。然而,这些结构的非对称EIT-like效应是由结构的拓扑决定的,一旦结构固定了,EIT-like效应的非对称响应情况也就固定了。为了实现灵活的EIT-like调控,亟须一种动态可调的单向EIT-like实现手段。

EIT-like效应可以通过在超材料中集成有源材料来实现动态调节。例如,通过外部电压或泵浦光激励,调节石墨烯的费米能级^[27-29]、二氧化钒薄膜(VO_2)^[30-31]和硅的电导率^[32-33],可以改变超材料中明暗/明明模式的分布或耦合情况,动态调控EIT-like透射/反射窗口。在微波系统中,Eleftheriades等^[34]提出一种基于微带线的有源超材料,在传统微带线上添加串联的变容二极管和并联的电感,组成复合左右手传输线(CRLH-TLs)超材料,该结构具有易于集成和加工、色

收稿日期: 2023-04-04; 修回日期: 2023-04-30; 录用日期: 2023-05-31; 网络首发日期: 2023-06-10

基金项目: 重庆市自然科学基金(cstc2020jcyj-msxmX0603)

通信作者: *ranjia@cqupt.edu.cn

散调节灵活等特点。本文基于该复合左右手传输线,利用外部偏置电压改变复合左右手传输线的电长度,从而原位动态调节微带谐振腔中的驻波场分布,最终改变腔体中基于 SRRs 结构的明、暗模式分布情况,实现激发端口可电切换的反射型单向 EIT-like 效应。这种激发端口可电切换的单向 EIT-like 效应有望为未来实现端口可切换的定向反射和多功能单向隐身器件提供新的解决方案。

2 仿真设计

所提激发端口可电切换的单向 EIT-like 结构如图 1(a) 所示,整体由 3 部分构成,包括中间的微带谐振腔、SRRs 和两边的 CRLH-TLs。微带谐振腔和 SRRs 如图 1(a) 蓝色虚线框所示,图 1(b) 是它的放大图。该谐振腔是由一条窄带高阻抗微带线和两端的低阻抗微带线所构成的法布里-珀罗(FP)腔,两个集成了电阻的 SRRs 呈旋转对称型,分布在谐振腔的上下两侧。两端的 CRLH-TLs 各由全同的 16 个单元构成,红色虚线框为其中的 3 个单元。CRLH-TLs 的放大图如图 1(c) 所示,其在微带线的基础上串联了变容二极管,同时并联了接地的电感,变容二极管通过

一个电感与外部偏置电压馈线相连。整体 EIT-like 结构的两端连接了 $50\ \Omega$ 的微带线。该结构采用厚度为 $1.57\ \text{mm}$ 的表面覆铜 Rogers RT5880 作为介质基底,介电常数 $\epsilon_r = 2.2$,损耗正切 $\tan \delta = 0.0009$ 。图 1(b) 中构成 FP 腔的微带线长度 L_{FP2} 为 $43.3\ \text{mm}$,宽 w 为 $0.2\ \text{mm}$ 。开口谐振环 SRRs 的长和宽为: $H = 6.5\ \text{mm}$ 、 $W = 4.8\ \text{mm}$ 。内环和外环的开口宽度 s_3 为 $0.2\ \text{mm}$,线宽 w 为 $0.2\ \text{mm}$,电阻值 R 为 $2.2\ \Omega$ 的两个贴片电阻集成在开口为 s_1 为 $0.6\ \text{mm}$ 的缝隙中。两个 SRRs 和微带线之间的间隔 s_2 均为 $0.2\ \text{mm}$,两者的中心到 FP 腔左端口的距离分别为: $X_1 = 15\ \text{mm}$ 、 $X_2 = 28.3\ \text{mm}$ 。在图 1(c) 所示的 CRLH-TLs 单元中,两种微带线的宽度 w_1 均为 $3\ \text{mm}$,长度分别为: $d_1 = 5\ \text{mm}$ 、 $d_2 = 1\ \text{mm}$,缝隙 $g = 0.8\ \text{mm}$,变容二极管的电容值记为 C_s ,电阻值 $R_s = 0.7\ \Omega$,如图 1(c) 中的绿色虚线所示,电感值 L_1 为 $4.7\ \text{nH}$ 的贴片电感通过孔连接到背面的接地铜膜。长度 d_3 为 $1\ \text{mm}$ 的微带线延伸到基底的上边沿,作为变容二极管的馈线网络,将外置偏压施加到变容二极管上。馈线长度 d_2 为 $1\ \text{mm}$ 的微带线通过一个电感值 L_2 为 $20.8\ \text{nH}$ 的电感相连接,以隔离高频信号。

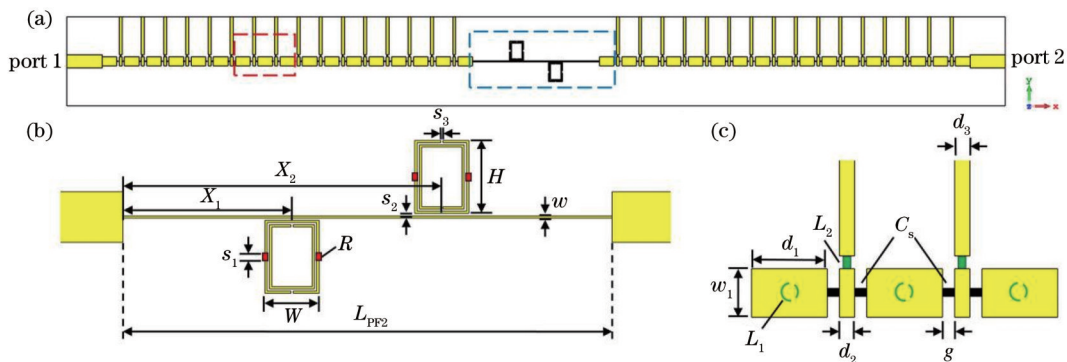


图 1 激发端口可电切换的非对称 EIT-like 结构示意图。(a) 整体结构示意图;(b) 图 1(a) 中蓝色虚线框局部放大图;(c) 图 1(a) 中红色虚线框局部放大图

Fig. 1 Schematic diagrams of asymmetric EIT-like structure with electrically switchable excitation port. (a) Overall structure diagram; (b) enlarged schematic of the part indicated by the blue dotted frame in Fig. 1 (a); (c) enlarged schematic of the part indicated by the red dotted frame in Fig. 1(a)

在外置偏压的作用下,串联变容二极管的电容值会发生改变,导致 CRLH-TLs 的传输特性发生变化。在仿真中,可以用不同的变容二极管电容值来模拟不同偏置电压所带来的影响。采用 CST Microwave Studio 来进行全波仿真分析。首先,在第 1 种情况(情况 I)下,将 FP 腔左端和右端的 CRLH-TLs 所有单元的变容二极管电容值都分别设置为 $2.5\ \text{pF}$ ($C_{\text{sl}} = 2.5\ \text{pF}$) 和 $1.5\ \text{pF}$ ($C_{\text{sr}} = 1.5\ \text{pF}$)。通过仿真分析可得到该复合结构的反射系数 $|S_{11}|$ 和 $|S_{22}|$,如图 2(a) 所示。从 2 端口(port 2)入射时,反射系数在接近 $3.97\ \text{GHz}$ 时出现一个极大值,此时 $|S_{22}|$ 为 0.538 ;而当入射端口改为 1 端口(port 1)时,在 $|S_{22}|$ 反射极大值频

点附近出现了一个反射谷,此时反射系数 $|S_{11}|$ 仅为 0.007 ,表明该结构在 $3.97\ \text{GHz}$ 出现了非对称的单向反射。只有从 2 端口入射时才会发生较强的反射,而从 1 端口入射时反射率几乎为 0,单向反射对比度 $\frac{||S_{11}| - |S_{22}||}{\max(|S_{11}|, |S_{22}|)}$ 达到 98.7% 。图 2(c) 是图 2(a) 中 $|S_{11}|$ 的群时延(group delay),可以看出,从 1 端口入射时,在 $3.97\ \text{GHz}$ 处产生了 $604\ \text{ns}$ 的群时延,出现了慢波效应。将 FP 腔左右两端 CRLH-TLs 中变容二极管的电容值交换,由于结构的对称性,在此情况下(情况 II),反射系数 $|S_{11}|$ 和 $|S_{22}|$ 的值发生了交换,如图 2(b) 所示,此时只有从 1 端口入射的波在 $3.97\ \text{GHz}$ 处会发生强反射,而从 2 端口入射时反射率接近为 0,且

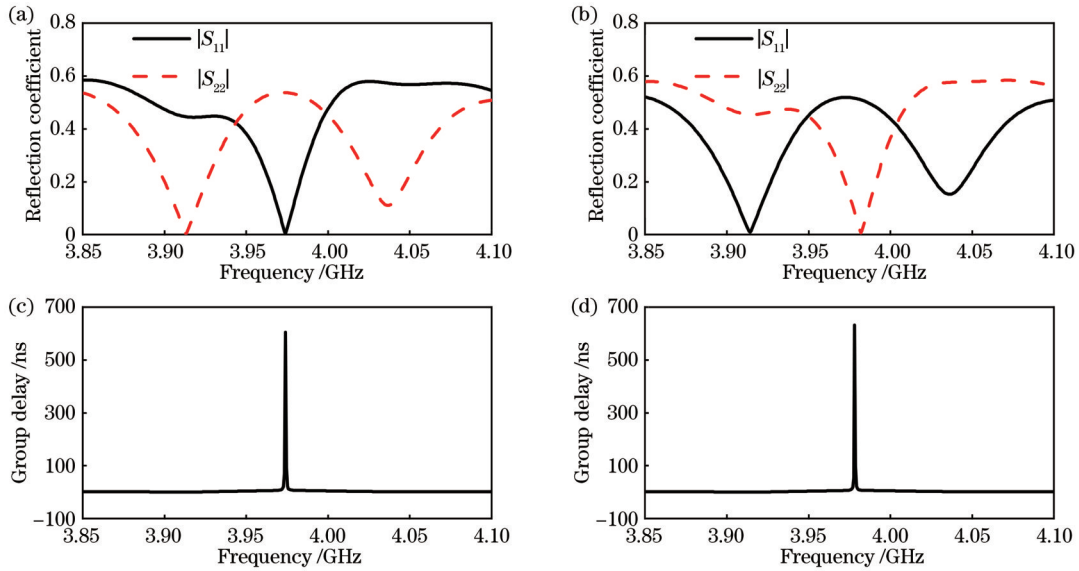


图 2 两种情况下激发端口可电切换的非对称 EIT-like 结构的反射系数及群延时。(a) 情况 I 的反射系数; (b) 情况 II 的反射系数; (c) 情况 I 时的 S_{11} 群时延曲线; (d) 情况 II 时的 S_{22} 群时延

Fig. 2 Reflection coefficients and group delays of asymmetric EIT-like structures with electrically switchable excitation port in two cases. (a) Reflection spectra of case I; (b) reflection spectra of case II; (c) group delays of S_{11} in case I; (d) group delays of S_{22} in Case II

由图 2(d) 可知, 2 端口入射时, 3.97 GHz 处出现了 632 ns 的群时延。

为了阐明这种单向反射端口可切换现象和慢波效应的物理机制, 对以上两种情况中的 CRLH-TLs 电磁特性及 FP 腔中的场分布进行详细分析。图 1(c) 中 CRLH-TLs 单元如图 3(a) 所示, CRLH-TLs 在不同变容二极管电容值 C_s 下的透射系数 $|S_{21}|$ 如图 3(b)、(c) 所示。可以看出, 随着 C_s 的改变, CRLH-TLs 在 3.97 GHz 的透射幅值较高, 维持在 0.75 附近, 但是透射相位随着 C_s 的增大会迅速减小。情况 I 时, 3.97 GHz 的透射幅值均大于 0.7, 透射相位分别接近 -180° 和 -90° , 两者电长度相差 90° 。将两种 CRLH-TLs 分别连接在 FP 腔的左右两端, FP 腔中的驻波场呈现非对称分布。此时 FP 腔中的磁场分布如图 4(a)、(c) 所示, 两个端口入射的波在 FP 腔中构筑的驻波场分布类似, 都有两个波节 (node) 和两个波腹 (antinode), 都呈现非对称分布状态。当考虑情况 II 时, 切换左右两边 CRLH-TLs 中变容二极管的电容值后, FP 腔中的磁场如图 4(b)、(d) 所示。对比图 4(a)、(b) 可知, 由于驻波场发生了 $1/4$ 波长的平移, FP 腔中的磁场强度分布发生了翻转, 原本波节 (波腹) 的位置变成了波腹 (波节), 对比图 4(c)、(d) 亦可知磁场分布情况发生了翻转。综上所述, 在情况 I 和情况 II 下, 两端 CRLH-TLs 对 FP 腔中的驻波场分布有翻转作用。

接下来, 进一步分析加载 SRRs 的 FP 腔中磁场的分布和近场耦合情况。由文献 [26] 可知, 入射波从某一端口入射时, 位于原波节处的 SRRs 与入射波的耦合强度小, 对 FP 腔的场分布影响也很小, 可以认为是

低损耗和高 Q 因子的暗模, 而位于波腹处的 SRRs 与入射电磁波发生了强耦合, 是一种具有大损耗和低 Q 因子的明模, 同时其会导致入射波发生强反射, 从而抑制电磁波继续传播到另一个端口, 并且会使得入射端口与该明模 SRRs 之间的磁场分布发生翻转。首先考虑情况 I ($C_{s1} = 2.5 \text{ pF}$, $C_{s2} = 1.5 \text{ pF}$) 时的电磁响应情况, 结果如图 4(a)、(c)、(e)、(g) 所示。对比图 4(a)、(e) 可知, 两个 SRRs 均位于 FP 腔的节点处。从图 4(e) 可以看出, 当 1 端口为入射端口时, 明模 SRRs 对驻波场的翻转作用增强了电磁波与原暗模 SRRs 的耦合强度, 激励起了暗模谐振, 暗模 SRRs 周围的磁场强度增大, 出现了 EIT-like 效应。然而, 当入射端口为 2 端口时, 如图 4(g) 所示, 明模 SRRs 翻转了其于 2 端口之间的磁场强度, 抑制了其于 1 端口之间的磁场, 因此暗模 SRRs 没有被激发, 此时没有发生 EIT-like 效应。以上结论能够很好地吻合图 2(a) 的结果, 表明在 3.97 GHz 处发生的单向反射现象和慢波效应是由于单向 EIT-like 效应导致的。

当切换左右两端的 CRLH-TLs 中变容二极管的电容值时, 对比图 4(e)、(f) 可知, 由于 FP 腔的磁场强度在 CRLH-TLs $1/4$ 波长的调制下发生了翻转, 原本处于空 FP 腔波腹 (波节) 的明模 (暗模) SRRs, 此时处于空 FP 腔的波节 (波腹) 处, 变成了暗模 (明模) SRRs。因此, 当从 1 端口入射电磁波时, 靠近 1 端口的明模 SRRs 对入射波发生了强反射, 最终暗模 SRRs 保持抑制状态, 不会和明模 SRRs 发生间接耦合, 没有产生 EIT-like 效应。然而, 当从 2 端口入射电磁波时, 明模 SRRs 翻转了其于 2 端口之间的磁场, 暗模 SRRs 被波腹处的强磁场激发, 产生了 EIT-like 效应, 如图 4(h) 所

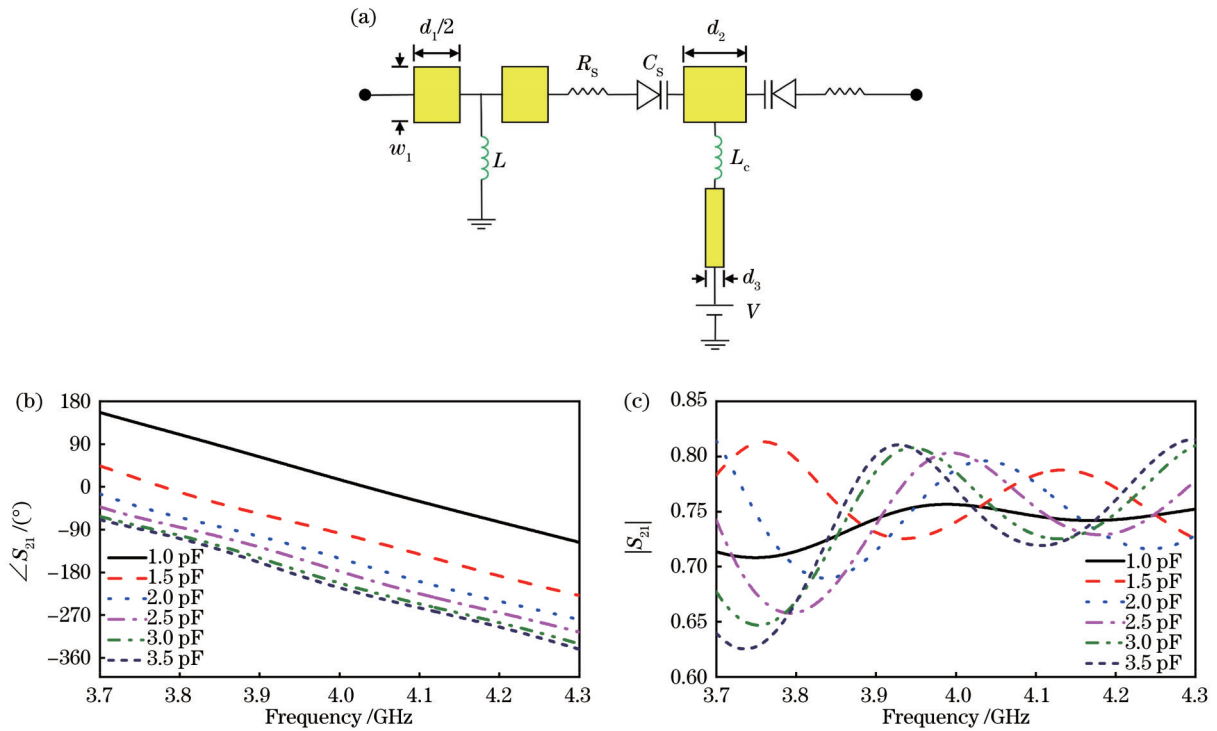


图 3 CRLH-TLs 单元示意图及传输特性。(a) CRLH-TLs 单元示意图；(b) 不同电容下 CRLH-TLs 透射相位；(c) 幅度
Fig. 3 Schematic and transmission characteristics of CRLH-TLs unit. (a) Schematic of the CRLH-TLs under different capacitance values; (c) amplitude

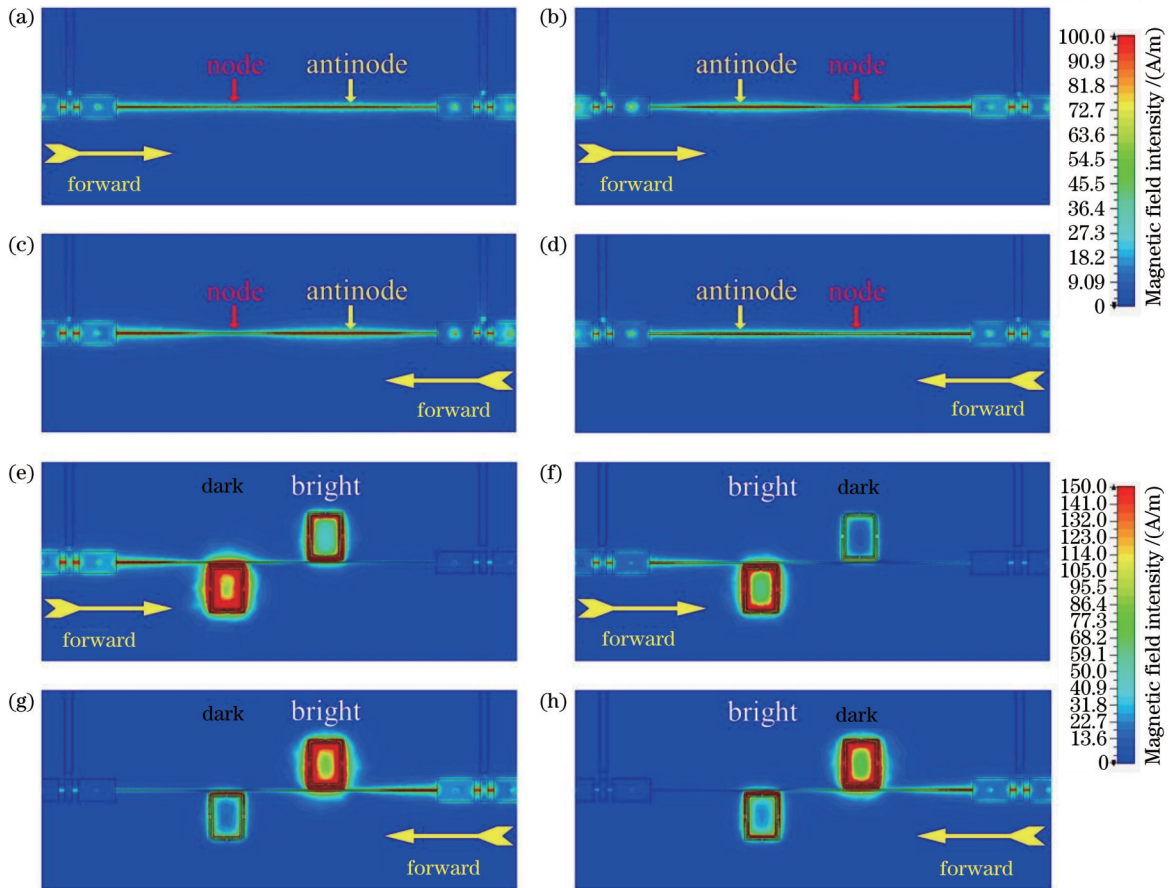


图 4 结构磁场分布图。(a)~(d) 空腔中 3.97 GHz 的磁场分布图；(e)~(f) 加入两个 SRRs 后 3.97 GHz 的磁场强度分布图
Fig. 4 Magnetic field distribution of the structures. (a)-(d) The simulated magnetic field distribution at 3.97 GHz in the bare cavity; (e)-(h) the simulated magnetic field distribution at 3.97 GHz in the cavity with two SRRs

示。因此与图 2(a)相比,图 2(b)的 $|S_{22}|$ 会出现反射谷和慢波效应,表明只有从 2 端口入射才会发生 EIT-like 效应,实现了单向 EIT-like 激发端口的切换。

综上所述,FP 腔中明模 SRRs 会根据入射端口来调控 FP 腔中的磁场,使其呈现出单向 EIT-like 效应,并且该效应的激发端口依赖于明模 SRRs 的位置。在此基础上,CRLH-TLs 在不同的电压/变容管容值下,电长度会发生 90° 的变化,导致 FP 腔中的磁场分布发生翻转,使得原本的明模 SRRs 变成暗模,而原本的暗模 SRRs 变成明模,如图 4(e)、(f)所示,最终明模 SRRs 位置的改变切换了单向 EIT-like 效应的激发端口。

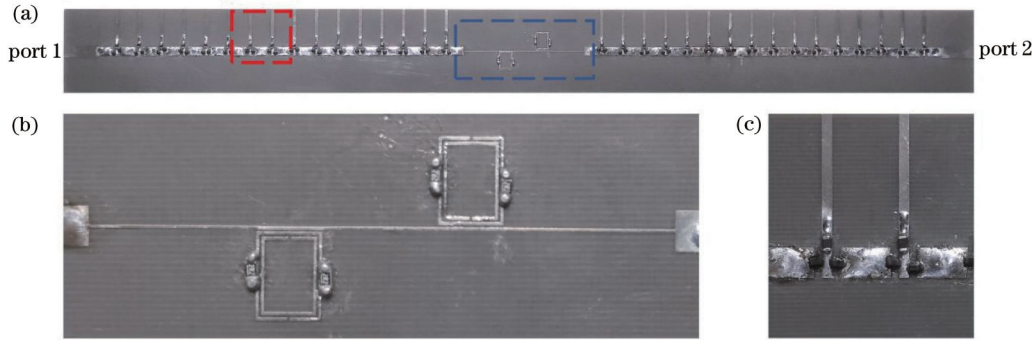


图 5 实验样品照片。(a)整体结构俯瞰图;(b)蓝色虚线框局部放大照片;(c)红色虚线框局部放大照片

Fig. 5 Photos of the sample. (a) Overview of the overall structure; (b) partial enlarged photo with blue dotted line frame in Fig. 5(a); (c) partial enlarged photo with red dotted line frame in Fig. 5(a)

测试时,FP 腔左边(右边)的 16 个 CRLH-TLs 单元施加的是相同的电压 V_1 (V_2)。图 6(a)是 V_2 固定为 0 V 时,反射系数 $|S_{11}|$ 随着 V_1 的变化情况。类似地,图 6(b)是 V_1 固定为 0 V 时,反射系数 $|S_{22}|$ 随着 V_2 的变化情况。从两幅子图可以看出,在两种情况下,偏压高于 6 V 时,3.4~3.9 GHz 之间的电磁波都被极大程度地反射,随着偏压的降低,反射变得越来越弱,最终出现一个反射极小的谷。图 6(c)同时展示了 $V_1 = 0$ V 和 $V_2 = 6$ V 时的反射系数 $|S_{11}|$ 和 $|S_{22}|$ 。由于变容管的容值随着偏压的增大而减小,因此此时 $C_{sl} > C_{sr}$,对应的是上一节提到的情况 I。图 6(c)中,此时 3.4~3.9 GHz 电磁波从 2 端口入射被大量反射,反射系数 $|S_{11}|$ 在 3.7 GHz 附近产生一个反射谷,并且其群时延在该频率达到了 15 ns。根据图 4 的分析可知,此时发生了反射型 EIT-like 效应。单向 EIT-like 效应伴随的非对称反射对比度达到 95.7%。将两端的 CRLH-TLs 的偏压值交换,即 $V_1 = 6$ V、 $V_2 = 0$ V,测得的反射谱如图 6(d)所示。此时 $C_{sl} < C_{sr}$,对应的是情况 II,即只有从 2 端口入射的电磁波才能激励起 EIT-like 效应, $|S_{22}|$ 在 3.4~3.9 GHz 附近有一个反射谷,而从 1 端口入射的电磁波在这个频率附近被大量反射,非对称反射对比度为 98.6%,EIT-like 波段的群

3 实验验证

根据图 1 所示的结构和参数,制作并测试了一个激发端口可电切换的单向 EIT-like 样品。样品照片如图 5(a)所示,其中,蓝色虚线框是 FP 腔和 SRRs,其放大图像如图 5(b)所示,红色虚线框中 CRLH-TLs 的放大照片如图 5(c)所示。变容二极管选用的 Skyworks 的 SMV1232-079LF,并联电感选用的 TDK 集总贴片电感,电感值为 4.7 nH。TDK 的磁珠 MPZ1608S601 TA00 被用作射频扼流器,替代电感 L_2 ,对射频信号实现抑制性扼流。SRRs 中的电阻 R 阻值为 2.2 Ω 。测试时采用直流电压源提供偏置电压,利用矢量网络分析仪测试样品的反射频谱。

时延也接近 20 ns。

以上测量结果表明,该非对称 EIT-like 效应的激发端口可以通过调节 CRLH-TLs 的偏置电压来实现动态切换,与第 2 节的仿真结果保持一致,但是中心频率略微有差别,造成这个差别的可能原因包括微带谐振腔和 SRRs 的加工精度、焊点对 SRRs 线宽的影响以及集总元件的非线性等,这些因素对 SRRs 的谐振频率产生较大的影响,从而对中心频率产生影响。

4 结 论

利用微带 FP 腔中的非对称驻波场与 SRRs 的相互作用,构造反射型的单向 EIT-like 效应,并利用加载变容二极管的有源 CRLH-TLs 灵活的电磁调控能力,对 FP 腔的驻波场分布实现动态翻转,最终实现激发端口可电切换的反射型单向 EIT-like 效应。该反射型单向 EIT-like 效应获得了 98.6% 的非对称反射对比度,改变偏置电压后,激励起 EIT-like 效应的端口发生切换,同时得到了 95.7% 的非对称反射对比度。这种激发端口可电切换的单向 EIT-like 弥补了目前非对称 EIT-like 效应研究工作的不足,有望运用于可原位动态调控的电磁波定向反射和多功能单向隐身器件中。

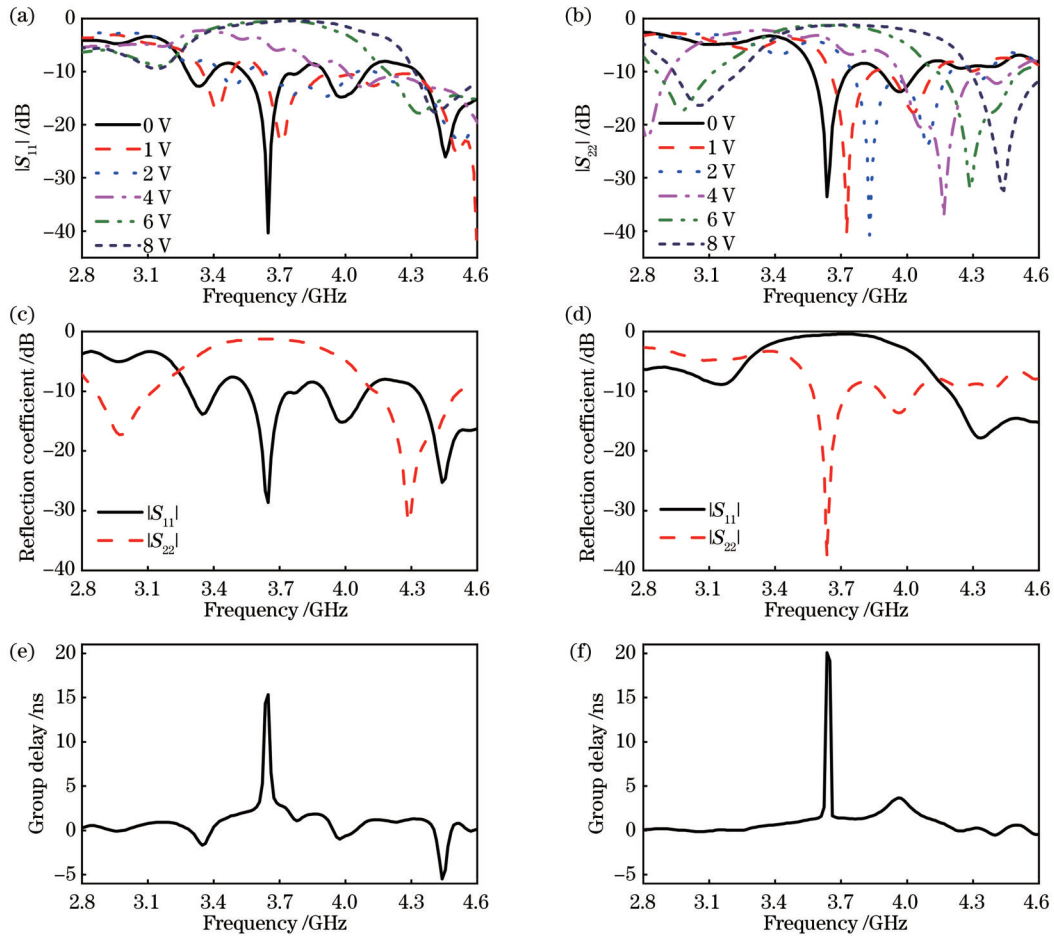


图 6 样品的反射谱及时延。(a) V_2 固定为 0 V 时, 不同 V_1 下反射系数 $|S_{11}|$; (b) V_1 固定为 0 V 时, 不同 V_2 下反射系数 $|S_{22}|$; (c) $V_1 = 0$ V、 $V_2 = 6$ V 时端口的反射系数 $|S_{11}|$ 和 $|S_{22}|$; (d) $V_1 = 6$ V、 $V_2 = 0$ V 时端口的反射系数 $|S_{11}|$ 和 $|S_{22}|$; (e) 对应图 6(c) 中 $|S_{11}|$ 的群时延曲线; (f) 对应图 6(d) 中 $|S_{22}|$ 的群时延曲线。

Fig. 6 Reflection spectra and group delay of the sample. (a) Measured $|S_{11}|$ of the metamaterial varying along with V_1 when V_2 is fixed as 0 V; (b) measured $|S_{22}|$ of the metamaterial varying along with V_2 when V_1 is fixed as 0 V; (c) measured $|S_{11}|$ and $|S_{22}|$ when $V_1 = 0$ V and $V_2 = 6$ V; (d) measured $|S_{11}|$ and $|S_{22}|$ when $V_1 = 6$ V and $V_2 = 0$ V; (e) group delay of $|S_{11}|$ in Fig. 6(c); (f) group delay of $|S_{22}|$ in Fig. 6(d)

参 考 文 献

- [1] Kasapi A, Jain M, Yin G Y, et al. Electromagnetically induced transparency: propagation dynamics[J]. Physical Review Letters, 1995, 74(13): 2447-2450.
- [2] Hain M, Stabel M, Halfmann T. Few-photon storage on a second timescale by electromagnetically induced transparency in a doped solid[J]. New Journal of Physics, 2022, 24(2): 023012.
- [3] Fan C Z, Ren P W, Jia Y L, et al. Highly tunable plasmon-induced transparency with Dirac semimetal metamaterials[J]. Chinese Physics B, 2021, 30(9): 096103.
- [4] Harris S E, Hau L V. Nonlinear optics at low light levels[J]. Physical Review Letters, 1999, 82(23): 4611-4614.
- [5] Wang C Q, Jiang X F, Zhao G M, et al. Electromagnetically induced transparency at a chiral exceptional point[J]. Nature Physics, 2020, 16(3): 334-340.
- [6] Bollinger K, Imamolu A, Harris S E. Observation of electromagnetically induced transparency[J]. Physical Review Letters, 1991, 66(20): 2593-2596.
- [7] Field J E, Hahn K H, Harris S E. Observation of electromagnetically induced transparency in collisionally broadened lead vapor[J]. Physical Review Letters, 1991, 67(22): 3062-3065.
- [8] Fan H R, Raza F, Ahmed I, et al. Three-type Fano interference controlled by the phase transition of $\text{Eu}^{3+}/\text{Pr}^{3+}:\text{YPO}_4$ [J]. New Journal of Physics, 2020, 22(9): 093008.
- [9] Zhang Y P, Wang Z G, Nie Z Q, et al. Four-wave mixing dipole soliton in laser-induced atomic gratings[J]. Physical Review Letters, 2011, 106(9): 093904.
- [10] Zhang S A, Genov D A, Wang Y A, et al. Plasmon-induced transparency in metamaterials[J]. Physical Review Letters, 2008, 101(4): 047401.
- [11] Lu H A, Liu X M, Mao D. Plasmonic analog of electromagnetically induced transparency in multi-nanoresonator-coupled waveguide systems[J]. Physical Review A, 2012, 85(5): 053803.
- [12] Lu H A, Gan X T, Mao D, et al. Graphene-supported manipulation of surface plasmon polaritons in metallic nanowaveguides[J]. Photonics Research, 2017, 5(3): 162-167.
- [13] Qin L, Zhang K, Peng R W, et al. Optical-magnetism-induced transparency in a metamaterial[J]. Physical Review B, 2013, 87(12): 125136.
- [14] Cao P F, Li C C, Li Y, et al. Electromagnetically induced transparency-like approach based on terahertz metamaterials for ultrasensitive refractive index sensors[J]. IEEE Sensors Journal,

- 2022, 22(3): 2110-2118.
- [15] Zhong J T, Xu X C, Lin Y S. Tunable terahertz metamaterial with electromagnetically induced transparency characteristic for sensing application[J]. *Nanomaterials*, 2021, 11(9): 2175.
- [16] Zhou T, Chen S G, Zhang X J, et al. Electromagnetically induced transparency based on a carbon nanotube film terahertz metasurface[J]. *Optics Express*, 2022, 30(9): 15436-15445.
- [17] Shen Z Y, Zhang Q H, Yang H L, et al. Analogy of multi-band electromagnetically induced transparency metamaterial based on simple combination of split-ring resonators[J]. *Applied Physics Express*, 2022, 15(7): 072007.
- [18] Wu Z L, An P Y, Ding M H, et al. Tunable electromagnetically induced transparent window of terahertz metamaterials and its sensing performance[J]. *Applied Sciences*, 2022, 12(14): 7057.
- [19] Zheng S Q, Ma M S, Lü Y, et al. Dual-band electromagnetically induced transparent metamaterial with slow light effect and energy storage[J]. *Journal of Physics D: Applied Physics*, 2022, 55(25): 255103.
- [20] Zografopoulos D C, Swillam M, Beccherelli R. Hybrid plasmonic modulators and filters based on electromagnetically induced transparency[J]. *IEEE Photonics Technology Letters*, 2016, 28(7): 818-821.
- [21] Hu Y Q, Xiong Y Q. High-Q and tunable analog of electromagnetically induced transparency in terahertz all-dielectric metamaterial[J]. *Applied Optics*, 2022, 61(6): 1500-1506.
- [22] Zhu L, Li T C, Zhang Z D, et al. Dual-band asymmetric transmission based on electromagnetically induced transparency (EIT) effect in a microstrip transmission line[J]. *Applied Physics A*, 2020, 126(4): 1-8.
- [23] Zhang Z R, Long Y, Zang X F. Unidirectional plasmonically induced transparency behavior in a compact graphene-based waveguide[J]. *Journal of Physics D: Applied Physics*, 2017, 50(29): 295301.
- [24] Zou X Y, Qiu D X, Yang H, et al. Dual-frequency unidirectional reflectionlessness in a non-Hermitian quantum system of two different energy-level quantum dots coupled to a plasmonic waveguide[J]. *Applied Physics B*, 2021, 127(12): 1-7.
- [25] Feng L, Xu Y L, Fegadolli W S, et al. Experimental demonstration of a unidirectional reflectionless parity-time metamaterial at optical frequencies[J]. *Nature Materials*, 2013, 12(2): 108-113.
- [26] Hu Y Y, Liu W X, Sun Y, et al. Electromagnetically-induced-transparency - like phenomenon with resonant meta-atoms in a cavity[J]. *Physical Review A*, 2015, 92(5): 053824.
- [27] Chen M M, Xiao Z Y, Lv F, et al. Dynamically tunable electromagnetically induced transparency-like effect in terahertz metamaterial based on graphene cross structures[J]. *IEEE Journal of Selected Topics in Quantum Electronics*, 2022, 28(1): 4700108.
- [28] 吕宇玲, 延凤平, 杜雪梅, 等. 偏振及角度不敏感类电磁诱导透明超材料研究[J]. *中国激光*, 2021, 48(23): 2314002.
- Lü Y L, Yan F P, Du X M, et al. Polarization- and angle-insensitive electromagnetically induced transparency-like metamaterial[J]. *Chinese Journal of Lasers*, 2021, 48(23): 2314002.
- [29] 刘姗姗, 李泉, 杨子榆, 等. 基于石墨烯-金属复合超材料结构的电磁诱导透明非线性调制[J]. *中国激光*, 2021, 48(19): 1918006.
- Liu S S, Li Q, Yang Z Y, et al. Nonlinear modulation of electromagnetically induced transparency based on graphene-metal hybrid metamaterial structure[J]. *Chinese Journal of Lasers*, 2021, 48(19): 1918006.
- [30] Chen M M, Xiao Z Y, Lu X J, et al. Dynamically tunable multi-resonance and polarization-insensitive electromagnetically induced transparency-like based on vanadium dioxide film[J]. *Optical Materials*, 2020, 102: 109811.
- [31] Ning R X, Xiao Z Q, Chen Z H, et al. Dual-tunable polarization insensitive electromagnetically induced transparency in metamaterials[J]. *Journal of Electronic Materials*, 2021, 50(7): 3916-3922.
- [32] 华沁怡, 陈心豪, 吕俊鹏, 等. 反射型太赫兹超表面电磁诱导透明效应[J]. *中国激光*, 2021, 48(12): 1214002.
- Hua Q Y, Chen X H, Lü J P, et al. Reflection-type electromagnetically induced transparency effect in terahertz metasurfaces[J]. *Chinese Journal of Lasers*, 2021, 48(12): 1214002.
- [33] 王娅茹, 梁兰菊, 杨茂生, 等. 一种光控的电磁诱导透明太赫兹超材料[J]. *激光与光电子学进展*, 2019, 56(4): 041603.
- Wang Y R, Liang L J, Yang M S, et al. Terahertz metamaterial based on controllable electromagnetic induced transparency structure[J]. *Laser & Optoelectronics Progress*, 2019, 56(4): 041603.
- [34] Eleftheriades G V, Iyer A K, Kremer P C. Planar negative refractive index media using periodically L-C loaded transmission lines[J]. *IEEE Transactions on Microwave Theory and Techniques*, 2002, 50(12): 2702-2712.

Unidirectional Electromagnetically Induced Transparency-Like Effect with Electrically Switchable Excitation Port

Ran Jia^{1,2,3*}, Zhang Siwen¹, Wang Wenchang¹, Hao Honggang^{1,3}, Tan Fei¹, Chen Yongqiang⁴

¹*School of Optoelectronic Engineering, Chongqing University of Posts and Telecommunications, Chongqing 400065, China;*

²*Postdoctoral Research Center of Chongqing Key Laboratory of Photoelectronic Information Sensing and Transmitting Technology, Chongqing University of Posts and Telecommunications, Chongqing 400065, China;*

³*Institute for Advanced Sciences, Chongqing University of Posts and Telecommunications, Chongqing 400065, China;*

⁴*School of Physical Science and Technology, Suzhou University of Science and Technology, Suzhou 215009, Jiangsu, China*

Abstract

Methods We take Rogers RT5880 copper-clad substrate with a thickness of 1.57 mm as the substrate of the microstrip cavity and CRLH-TLs. The thickness of the copper layer is 0.035 mm. A Fabry-Perot (FP) cavity is formed inside a microstrip line. Two SRRs are placed in the cavity and located at the antinode and node of the electromagnetic field in the FP cavity respectively to construct a unidirectional EIT-like structure. The excitation port of the EIT-like effect is determined by the sequence of the antinode and node in the FP cavity. Tunable composite right/left-handed transmission lines (CRLH-TLs) loaded with varactors are added at the two ends of the FP cavity (marked as left and right CRLH-TLs respectively) to change the electromagnetic field distribution in the cavity. By optimizing all parameters, the electrical lengths of CRLH-TLs are quarter wavelength and half wavelength respectively under different bias voltages. Therefore, since the distribution of the nodes and antinodes in the cavity can be switched by changing the electric length of the CRLH-TLs, the sequence of the antinode and node where the two split ring resonators (SRRs) lie in the cavity is also switched, which leads to a switched EIT-like excitation port. Finally, a sample is fabricated and tested to validate the unidirectional EIT-like effect with the electrically switchable excitation port.

Results and Discussions This structure realizes the unidirectional EIT-like effect to bring a unidirectional reflection with high contrast ratio. It is validated both in simulation and experiments that the contrast ratio of the unidirectional reflection can reach more than 95%, and the excitation port of the unidirectional EIT-like effect is determined by the sequence of nodes and antinodes in the FP cavity. The capacitance of the varactors in the CRLH-TLs varies along with the bias voltage. Thus, different bias voltages are simulated by setting different capacitance values. In case I, the capacitance of varactors in the left CRLH-TLs is set as 2.5 pF ($C_{sl} = 2.5$ pF) and that in the right is set as 1.5 pF ($C_{sr} = 1.5$ pF). The magnitude of the reflection coefficient of port 1 $|S_{11}|$ and port 2 $|S_{22}|$ at 3.97 GHz are 0.007 and 0.538 respectively, showing that the EIT-like effect is only excited through port 1. Case II has swapped the capacitance of the varactors in the right and left CRLH-TLs units. Thus the reflection spectra $|S_{11}|$ and $|S_{22}|$ will also be exchanged due to the geometric symmetry of the switchable EIT-like effect. At last, the excitation port of the EIT-like effect has been switched to port 2, indicating that switching the bias voltage can achieve a unidirectional EIT-like effect with an electrically switchable excitation port (Fig. 2). When the capacitance of the varactors is set as 1.5 pF and 2.5 pF, the transmission amplitudes of the CRLH-TLs are both larger than 0.7 and $\angle S_{21}$ are close to -90° and -180° at 3.97 GHz respectively (Fig. 3). Since the transmission phase difference between the CRLH-TLs units with the capacitance of 2.5 pF and 1.5 pF is -90° , once the capacitance of the varactors in the left and right CRLH-TLs is exchanged, the sequence of the nodes and antinodes in the FP cavity is reversed. As a result, the port to excite the unidirectional EIT-like effect is switched (Fig. 4). For the fabricated sample, when the bias voltage on the left and right sides of the CRLH-TLs are $V_1 = 0$ V and $V_2 = 6$ V respectively, only when the wave is incident from port 1, the EIT-like effect can be excited. Through exchanging the bias voltages, the unidirectional EIT-like excitation port is switched. This shows that the structure can achieve a unidirectional EIT-like effect with an electrically switchable excitation port.

Objective Unidirectional electromagnetically induced transparency-like effect is a special kind of EIT-like effect, which is caused by its asymmetric structure. The EIT-like effect can be excited by the asymmetric structure only when a wave is incident from a certain port. The unidirectional EIT-like effect plays a significant role in realizing directional reflection and transmission and is crucial in unidirectional invisibility. With the development of tunable metamaterials, various kinds of reconfigurable metamaterials are also proposed to realize a tunable EIT-like effect. However, the dynamically switchable

unidirectional EIT-like effect has been barely reported. The excitation port of the unidirectional EIT-like effect is usually fixed and determined by the structure topology. To realize a reflection-type unidirectional EIT-like effect, an electrically switchable excitation port based on tunable CRLH-TLs and a two-port microstrip cavity embedded with two SRRs is proposed. The reflection-type EIT-like effect can only be excited when an electromagnetic wave is incident from a certain port. The contrast ratio of the asymmetric reflection coefficient of the two ports in our paper reaches 98.7%. On this basis, the coupling between the microstrip cavity and the SRRs is dynamically modulated by the tunable CRLH-TLs, thereby changing the excitation port of the unidirectional EIT-like effect. Finally, a unidirectional EIT-like effect with an electrically switchable excitation port is achieved, and the applications of the EIT-like effect in optical storage, optical modulation, sensing, and other fields are promoted.

Conclusions We propose a reflection-type unidirectional EIT-like effect with an electrically switchable excitation port, and validate it in simulation and experiments. To switch the excitation port of the unidirectional EIT-like effect, our paper reverses the sequence of nodes and antinodes in the FP cavity by changing the bias voltages of CRLH-TLs on both sides of the cavity. This unidirectional EIT-like effect with an electrically switchable excitation port provides a feasible scheme for tunable asymmetric EIT-like effects and is expected to be applied in directional reflection and multifunctional unidirectional stealth devices.

Key words electromagnetically induced transparency-like; composite right/left-handed transmission lines; microstrip cavity; split ring resonators; unidirectional reflection